



Soil organic carbon accrual due to more efficient microbial utilization of plant inputs at greater long-term soil moisture

Itamar A. Shabtai^{a,*}, Srabani Das^b, Thiago M. Inagaki^{c,1}, Behrooz Azimzadeh^a,
Brian Richards^d, Carmen Enid Martínez^a, Ingrid Kögel-Knabner^{c,f},
Johannes Lehmann^{a,e}

^a Soil and Crop Sciences, School of Integrative Plant Science, Cornell University, Ithaca, NY 14850, USA

^b Center for Carbon Management and Sequestration, The Ohio State University, Columbus, OH 43210, USA

^c Chair of Soil Science, School of Life Sciences, Technical University of Munich, 85354 Freising, Germany

^d Biological and Environmental Engineering, Cornell University, Ithaca, NY 14850, USA

^e Cornell Atkinson Center for Sustainability, Cornell University, Ithaca, NY 14850, USA

^f Institute for Advanced Study, Technical University of Munich, Lichtenbergstraße 2a, 85748 Garching, Germany

Received 14 March 2022; accepted in revised form 26 April 2022; Available online 30 April 2022

Abstract

High long-term soil moisture may either stimulate or inhibit soil organic carbon (SOC) losses through changes to mineral and chemical composition, and resultant organo-mineral interactions. Yet, the trade-off between mineralization and accrual of SOC under long-term variation in unsaturated soil moisture remains uncertain. We tested the underexplored relationships between long-term soil moisture and organo-mineral chemical composition and its implications for SOC persistence in an experimental field in New York, USA, with differences in long-term mean soil volumetric water content (0–0.15 m depth) ranging from 0.40 to 0.63 (v/v) during the growing season. Long-term soil moisture across 20 subplots on four fallow plots were positively correlated with SOC ($R^2 = 0.23$; $P = 0.019$, $n = 20$), mineral-associated organic matter (MAOM) content (g fraction/g soil) ($R^2 = 0.44$; $P = 0.001$; $n = 20$) and occluded particulate organic matter (oPOM) content ($R^2 = 0.18$; $P = 0.033$; $n = 20$). Higher long-term soil moisture was associated with a decrease in the relative content of sodium pyrophosphate extractable Fe ($R^2 = 0.33$; $P < 0.005$; $n = 20$), an increase in sodium dithionite extractable Fe ($R^2 = 0.44$; $P < 0.001$; $n = 20$), and an increase in SOC retention by non-crystalline Al pools ($R^2 = 0.51$; $P = 0.0002$ for sodium pyrophosphate extracts, $R^2 = 0.41$; $P = 0.0014$ for hydroxylamine hydrochloride extracts; $n = 20$ for both). Increasing long-term soil moisture was associated with a four-fold increase in microbial biomass C (per unit SOC) and lower metabolic quotient ($R^2 = 0.56$, $P < 0.001$). MAOM fractions of high-moisture soils had lower C:N (from C:N 9.5 to 9.0, $R^2 = 0.27$, $P = 0.011$, $n = 20$). Consistent with decreasing C:N, increasing decomposition with increasing moisture was reflected by a 15% and 10% greater proportion of oxidized carboxylic-C to aromatic-C and O-alkyl C, respectively, as measured with ^{13}C NMR, and a more pronounced FTIR signature of N-containing proteinaceous compounds in high-moisture MAOM fractions, indicative of microbial metabolites and transformation products. A partial least squares regression showed that SOC content increased with greater long-term moisture ($P = 0.019$), pyrophosphate-extractable Al ($P = 0.0001$), and exchangeable Ca

* Corresponding author at: Department of Environmental Sciences, The Connecticut Agricultural Experiment Station, New Haven, CT 06504-1106, USA.

E-mail address: itamar.shabtai@ct.gov (I.A. Shabtai).

¹ Current address: Norwegian Institute of Bioeconomy Research (NIBIO), Department of Biogeochemistry and Soil Quality, Høgskoleveien 7, 1430 Ås, Norway.

($P = 0.013$). Taken together, our results show that higher long-term soil moisture resulted in SOC accrual by enhancing conversion of plant inputs into microbial biomass that interacts with reactive minerals.

© 2022 Elsevier Ltd. All rights reserved.

Keywords: Soil organic carbon; Long-term soil moisture; Microbial carbon cycling; Organo-mineral interactions; Metabolic quotient

1. INTRODUCTION

Soils comprise the largest terrestrial store of organic carbon (OC) (Friedlingstein et al., 2019) and play a substantial role in the global C cycle (Scharlemann et al., 2014). As a result, increasing soil organic carbon (SOC) storage by decreasing losses to CO₂ may be a feasible strategy to withdraw atmospheric CO₂ and partially offset anthropogenic emissions driving climate change (Minasny et al., 2017). As climate change is expected to drastically alter soil moisture conditions globally (Seneviratne et al., 2010; Grillakis, 2019), a better understanding of the trade-off between SOC mineralization and stabilization under long-term changes to soil moisture is needed to manage SOC stocks (Falloon et al., 2011). Importantly, unlike soil temperature, which is expected to rise and increase SOC mineralization (Soong et al., 2021), soil moisture is a parameter that can be managed – through irrigation, controlled drainage, and wetland restoration – and can indirectly curb soil warming through evapotranspiration (Seneviratne et al., 2010).

Soil moisture controls SOC turnover and storage by regulating fundamental processes such as biotic activity (Moyano et al., 2013), solute transport, gaseous exchange, and mineral weathering (Schjønning et al., 2003; Moyano et al., 2013; Kramer and Chadwick, 2018). Short-term increases in soil moisture are known to stimulate microbial activity (Ghezzehei et al., 2019), yet long-term increases may either stimulate or decrease SOC losses by changes to vegetation (Chen et al., 2020b), mineral composition (Doetterl et al., 2015; Khomo et al., 2017), SOC chemical composition (Hall et al., 2018) and resultant organo-mineral interactions (Mikutta et al., 2009; Kramer et al., 2012). Most studies evaluate broad gradients in precipitation, soil mineral properties, or soil age, which inevitably interact in complex ways. Yet, the direct effects of long-term differences in soil moisture on SOC turnover have received little attention (Moyano et al., 2013), largely due to the challenge of isolating measurable variation in long-term soil moisture at field scale. This has limited our ability to predict and manage SOC stocks in the face of changing soil moisture conditions (Todd-Brown et al., 2014; Berg and Sheffield, 2018).

SOC is widely considered to consist of microbial residues and necromass (Schurig et al., 2013; Zhu et al., 2020) which have been protected from further decomposition through interactions with the mineral matrix (Kleber et al., 2021). Therefore, SOC turnover is largely dependent on the efficiency of microbial conversion of organic inputs into microbial biomass (i.e., substrate use efficiency), with greater efficiency indicative of greater C storage in the soil as microbial biomass (Manzoni et al., 2012) and mineral-associated SOC (Zhu et al., 2020). Long-term soil moisture

comes into play by regulating diffusion rates of substrates used by microbes (Butcher et al., 2020). Low water content inhibits diffusion of dissolved compounds in the soil solution due to thinning of water films in soil pores, and increased flow path length and solution viscosity (Butcher et al., 2020), thus limiting the probability of encounters between microbes, extracellular enzymes, and substrates. Recent work has shown that limited substrate diffusion at low soil water contents can decrease microbial carbon use efficiency (Butcher et al., 2020). Additionally, increased microbial activity at high moisture conditions can enhance the conversion of high molecular weight, hydrophobic plant inputs into soluble, charge-containing, low molecular weight compounds, which tend to interact with mineral surfaces (Lehmann and Kleber, 2015). Thus, SOC cycled under greater long-term soil moisture may have greater persistence and result in net SOC accrual, yet experimental evidence is lacking.

The amount and nature of soil minerals often control the content, composition, and persistence of adsorbed or occluded SOC (Sanderman et al., 2014; Rasmussen et al., 2018; Kleber et al., 2021). SOC may predominantly interact with non-crystalline or crystalline Fe and Al oxide phases, or with phyllosilicate clay minerals and their exchangeable cation (e.g., Ca), depending on their type and relative content in the soil (Hall et al., 2018; Khomo et al., 2017; Mikutta et al., 2006; Rowley et al., 2018; Singh et al., 2017). Furthermore, long-term differences in soil moisture can result in different rates of chemical weathering of minerals, which can alter their reactivity and capacity to retain SOC, with implications for SOC stabilization (Doetterl et al., 2015). For example, greater long-term moisture may lead to abiotic or biotic reduction of Fe in non-crystalline phases, resulting in increased crystallinity (Thompson et al., 2006) and release of Fe-associated C (Huang and Hall, 2017). Fe loss across a rainfall gradient has been shown to increase the relative importance of Al oxide phases (which are not redox sensitive) for retaining SOC (Inagaki et al., 2020). However, the effects of mineral composition on organo-mineral interactions across large geographical gradients may be confounded by other factors such as climate and vegetation. Therefore, we studied the effects of increasing long-term soil moisture under unsaturated conditions at field scale to isolate soil moisture as an explanatory variable for microbial turnover of SOC, SOC storage in soil density fractions, and the chemical composition of organo-mineral associations. We then determined how the variables that were affected by long-term moisture influenced SOC amount, and SOC mineralization in laboratory incubations. We hypothesized that (1) soils experiencing greater long-term moisture will have more oxidized SOC functional groups and greater relative

contents of non-crystalline Al phases due to greater organic decomposition and mineral weathering, respectively, and (2) that increased reactivity of SOC functional groups and oxides will enhance organo-mineral interactions in high-moisture soils which will increase SOC persistence leading to SOC accrual.

2. MATERIALS AND METHODS

2.1. Field site

The field site was located near Ithaca, New York, USA (42N28.20', 76W25.94') and included a drainage catena of three primary soil series: well-drained Canaseraga (coarse-silty, mixed, active, mesic typic Fragiudept), slightly poorly drained Dalton (Coarse-silty, mixed, active, mesic aeris Fragiaquept) and poorly drained Madalin (fine, illitic, mesic mollic Endoaqualf) (Das et al., 2018). The epipedon texture is primarily silt loam, characterized by dense subsoil fragipans and recurring perched water tables resulting from the restrictive subsoil layers. The field topography is undulating, with slopes varying from 0 to 8% (and a small area with short slopes of up to 15% on the eastern edge). The mean annual temperature and precipitation at the site are 10 °C and 940 mm, respectively.

The field has not been plowed since at least 1954 (as indicated from aerial photos). Since then, it has been under perennial grass and broadleaf forbs cover and has been mowed every several years. The field has been wholly fallowed since 2005. In June 2011, a perennial grass bioenergy crop field experiment was set up, and four fallow plots were used as a control for different cropping systems. All the plots (fallow and perennial grasses) were laid out to capture the range of soil moisture regimes, varying from moderately well-drained to poorly drained (Das et al., 2019). Here, we studied soils sampled from five sampling subplots within each of the four fallow plots (thus $n = 20$). The characteristic soil moisture regime along the four fallow plots was previously determined following a soil moisture measurement campaign carried out from 2011 to 2015 (Das et al., 2018) (See Fig. S2 for 2011–2018 data). The volumetric water content of each sampling site's surface layer was measured via replicated time-domain reflectometry (TDR). The relative soil water content was determined by dividing the sample location's volumetric water content by the mean field value for each sampling event. For each of the over 40 sampling events, a normalized growing season moisture value was calculated for each of 80 sampling sites (including the 20 fallow sites and 60 other non-fallow sites not reported here) based on the multi-year mean of its relative water content. Thus, the multi-year mean cumulatively represents several thousand readings at the field (Das et al., 2018). The normalized moisture values were binned into quintiles (Das et al., 2018) (Table S1). The wettest subplots (denoted as Q1) had the highest water contents relative to the field mean, and the driest subplots (denoted as Q5) had the lowest water contents relative to the field mean.

At the time of sampling, the plant cover consisted of fallow (unmowed for circa 10 years) grasses dominated by legacy reed canarygrass (*Phalaris arundinacea* L.)

interspersed with numerous other grasses and broadleaf forbs. The plots were undisturbed aside from small (1 m²) hand harvests at subplots after dormancy to characterize yields for comparison with other cropping treatments.

2.2. Sampling method

An overview of the experimental design is presented in Fig. S1. Soils were sampled from the surface Ap layer (0–0.15 m depth) in October 2018 at two locations equidistant (1.2 m) from the center of each of the 20 sampling points (marked by a permanent flag). Approximately two kg of soil were dug from each location, composited in a bucket, mixed, and transported to the lab in a cooler. One half of each sample was air-dried and passed through a 2 mm sieve, and one half was passed through a 4 mm sieve and stored at –20 °C for microbial biomass and soil respiration analyses. Visible rocks and plant material were removed from each sample. Composited samples, prepared by combining equal amounts of the soils from quintiles Q1, Q3, and Q5 (Table S1), were used for ¹³C NMR and C NEXAFS analyses. These composited samples are referred to as High moisture, Mid moisture, and Low moisture, respectively. Aboveground and belowground biomass were sampled annually during 2013–2020 and 2013–2015, respectively, as described (Das et al., 2019). Since biomass was not different across the moisture gradient, we conclude that organic input amounts were also similar across normalized moisture values in the fallow plots (Fig. S7).

2.3. Soil analyses

2.3.1. Soil characterization

Gravimetric and hygroscopic water contents were determined on field moist and air-dry samples, respectively, after drying to constant weight at 105 °C. Water filled pore space was calculated by determining the gravimetric soil water content at saturation, as described (DeCiucies et al., 2018). Soil pH was measured on 1:2.5 soil:deionized water extractions. Exchangeable cations were extracted using 1 N ammonium acetate at pH 7 and measured on an inductively coupled plasma spectrometer (Thermo iCAP 6000 series). Exchangeable Ca (Ca_{EX}) and pH increased with normalized moisture values (Fig. S15), as reported (Das et al., 2018; Das et al., 2019).

2.3.2. Soil fractionation

We used a combination of size and density fractionation to isolate operationally defined – but ecologically relevant – fractions. Soil samples (10 g) were gently agitated for 10 s with 35 mL of sodium polytungstate (SPT) adjusted to a density of 1.65 Mg m⁻³. The samples were left to settle overnight, centrifuged (3000 RCF, 30 min), filtered (GF/F, 0.7 μm glass fiber filter), and washed with 500 mL of deionized water. The obtained material is referred to as free particulate organic matter (fPOM). New SPT solution (35 mL, 1.65 Mg m⁻³) was added to the samples, and a vortex was used to re-disperse the soil. The samples were sonicated (XL 2020, QSonica, Newtown, CT, USA) at 350 J mL⁻¹ of energy (operated at 75 J s⁻¹), left overnight

to allow the particles to settle, and centrifuged (3000 RCF, 45 min). The floating material, referred to as occluded particulate organic matter (oPOM), was isolated as described above. The remaining pellet was washed with deionized water and centrifuged (3000 RCF, 30 min) three times to remove the SPT (final supernatant density was $1 \pm 0.02 \text{ M g m}^{-3}$). Next, the soils were shaken end-to-end with sodium hexametaphosphate (35 mL, 0.5% w/v) for 16 hours and wet sieved (53 μm) to separate the sand-sized fraction (material remaining on the sieve) from the silt and clay size fractions (material passing the sieve). The material passing the sieve was referred to as the mineral-associated organic matter (MAOM) fraction. The MAOM and sand fractions were transferred to a pre-tared aluminum tin and dried at 60 °C. The four obtained fractions – fPOM, oPOM, MAOM, and sand – were weighed, ball-milled (except the sand), and stored. Total C, N, and isotope ratios of the fractions (except the sand) and bulk soil samples were measured using a Delta V Isotope Ratio Mass Spectrometer (Thermo Scientific, Germany) coupled to a Carlo Erba NC2500 Elemental Analyzer. We assumed total C equaled organic C since these soils did not contain carbonates (Das et al., 2018) and their pH was <7. The mean mass recovery was 102%. C recovery ranged from 96 to 109%, and N recovery ranged from 98 to 106%. Sand was assumed to contain zero C and N based on measurements of representative sand samples. The average C content in fPOM and oPOM were 35% and 25%, respectively, indicating that minerals were present in these fractions. We present results from density fractionation in two ways: 1. mass of fraction per unit mass soil (g fraction/100 g soil) and 2. amount of fraction C per unit total C in the soil (mg fraction C/g SOC).

2.3.3. Oxide extraction

We performed a sequential oxide extraction following a modified protocol (Heckman et al., 2018) using sodium pyrophosphate (PY), hydroxylamine hydrochloride (HH), and sodium dithionite (DITH) to sequentially release SOC retained by different phases of soil Al and Fe. Based on published extraction protocols (Ross et al., 1985; Parfitt and Childs, 1988; Wagai and Mayer, 2007; Courchesne and Turmel, 2007; Heckman et al., 2018), we assume that PY extracts organically complexed Al and Fe, HH extracts non-crystalline inorganic Fe including ferrihydrite, and DITH extracts crystalline Fe phases like goethite, hematite, and lepidocrocite.

We acknowledge that Al and Fe released by PY, HH, and DITH extractions approximately correspond to specific phases as these extractions are not perfectly selective (Parfitt and Childs, 1988; Kaiser and Zech, 1996). We cannot rule out that PY-extractable Fe and Al were free of colloidal material caused by the alkalinity (pH 10) of the extracting solution, however, this effect is most pronounced in tropical soils with >40% clay content (Schuppli et al., 1983), while our temperate soils contained <25% clay. Furthermore, we acknowledge that the dithionite extraction may liberate C associated with silicate clay (Wang et al., 2021). Despite these caveats, inorganic oxide extractions remain an important and widely-used approach to study

the impact of Al and Fe phases on SOC storage and turnover times (Masiello et al., 2004; Zhao et al., 2016; Porras et al., 2017; Wagai et al., 2020; Wang et al., 2021).

Briefly, sodium pyrophosphate (25 mL, 0.1 M), hydroxylamine hydrochloride (25 mL, 0.1 M prepared in 0.25 M HCl), and sodium dithionite (30 mL, 0.05 M) were sequentially added to soil samples (0.1 g), shaken for 16 hours, centrifuged (3000 RPM, 1 hour), and the clear supernatant was passed through glass fiber filter papers (0.45 μm , Advantec). Following extraction with sodium dithionite, soils were shaken for one hour with an HCl solution (10 mL, 0.05 M) which was combined with the sodium dithionite extract (Heckman et al., 2018). The concentration of dissolved Fe and Al was measured by an inductively coupled plasma spectrometer (Thermo iCAP 6000 series). The concentration of OC in each extract, considered the C associated with Al and Fe, was measured by combustion catalytic oxidation (TOC-VCPN TOC analyzer, Shimadzu, Japan).

2.3.4. Microbial biomass carbon

Microbial biomass C was measured following the chloroform-fumigation-extraction method (Witt et al., 2000). Briefly, ethanol-free chloroform (4 mL) was added to 10 g of field moist soil (<4 mm) in stoppered 250 mL Erlenmeyer flasks. The samples were incubated for 24 hours, after which the flasks were vented in a fume hood until the chloroform had fully evaporated. Fumigated and non-fumigated soils were agitated for 1 hour with K_2SO_4 (0.05 M, 50 mL) and filtered through No. 1 Whatman paper. The total extractable organic C was measured by combustion catalytic oxidation (TOC-VCPN TOC analyzer Shimadzu, Japan). Microbial biomass C was calculated as the difference between paired chloroform-fumigated and non-fumigated subsamples, after correcting for sample water content. Dissolved organic C (DOC) was determined as the C extracted from the non-fumigated samples.

2.4. Spectroscopic studies

2.4.1. Fourier Transform Infrared (FTIR) spectroscopy

FTIR spectra were collected on a Vertex 70 spectrometer (Bruker Corp., Billerica, MA) equipped with an ATR sampling accessory (GladiATR, Pike Technologies, Madison, WI). Spectra were collected on dry (60 °C) ball-milled samples ($n = 20$) of soils, MAOM, fPOM, and oPOM fractions, and on ashed (500 °C for 3 h) MAOM samples. Spectra representing an average of 64 scans were collected from 450 to 4500 cm^{-1} at a resolution of 4 cm^{-1} . Replicate spectra for each sample ($n = 3$) were baseline corrected, normalized, and averaged. To identify features originating from organic constituents, spectra of ashed MAOM were subtracted from non-ashed MAOM samples and smoothed (17-point Savitsky-Golay smoothing). Spectral processing was performed using the OPUS 7.2 software (Bruker Corp., Billerica, MA). Our spectral analysis focused on the wavenumber ranges 2800–3800 and 1300–1800 cm^{-1} , which contain information on organic and inorganic components (see Section 3.4). Negative absorbance values between 1150 and 1250 cm^{-1} precluded

analysis of this spectral range. ATR-FTIR vibrational assignments of organic and inorganic constituents were based on previous publications (Lehmann et al., 2007; Parikh et al., 2014; Fine et al., 2018).

2.4.2. ^{13}C Nuclear Magnetic Resonance (NMR)

The molecular structure of organic matter in the bulk soil and soil fractions was analyzed using ^{13}C NMR spectroscopy (Biospin DSX 200 NMR spectrometer, Bruker, Rheinstetten, Germany) with a contact time of 0.001 sec with a pulse delay of 0.4 sec for bulk soil and silt and clay fractions, and 1 sec for fPOM and oPOM fractions. At least 100,000 accumulated scans were performed. The spectra were integrated using four major chemical shift regions: 0–45 ppm (alkyl-C), 45–110 ppm (O/N-alkyl-C), 110–160 (aryl-C), and 160–220 ppm (carboxyl-C) (Knicker and Lüdemann, 1995). Sample pre-treatment with hydrofluoric acid was not necessary to obtain a well-resolved spectrum. We applied a molecular mixing model (Nelson and Baldock, 2005) to estimate the proportions of biochemical component equivalents from ^{13}C NMR spectral regions and N:C ratios. The biochemical components of the model are carbohydrate, protein, lignin, lipid, char, and carbonyl.

2.4.3. Carbon K-edge Near Edge X-Ray Absorption Fine Structure (NEXAFS)

SOC chemical composition in bulk soil and soil fractions was analyzed with C K-edge NEXAFS collected at the spherical grating monochromator (SGM) beamline of the Canadian Light Source (Saskatoon, SK). The beamline is equipped with a silicon drift detector for partial fluorescence yield (PFY). Samples were deposited on gold (Au)-coated silicon wafers and air-dried. PFY scans (60 s) were collected with an $\sim 50 \times 50 \mu\text{m}$ probe in slew mode. The PFY with maximum C signal (detector 90° to incident beam) was normalized to the PFY scattering signal from a clean Au-coated Si wafer to account for in-line C contamination. The spectra were edge-normalized (edge step = 1) and flattened in Athena (Demeter 0.9.25) (Ravel and Newville, 2005). SOC composition was assessed by comparing peak height ratios of the three primary spectral features: aromatic (C=C) at ~ 285.6 eV, substituted aromatic (e.g., C=C–OH) at ~ 286.7 eV, and carboxylic (C=O–OH) at ~ 288.7 eV (Solomon et al., 2009; Heymann et al., 2011). Peak heights were determined by the Gaussian function fitting algorithm in Fityk v. 1.3.1 (Wojdyr, 2010), identifying the maximum of a Gaussian function of full-width half maximum (FWHM) = 0.6 eV (Possinger et al., 2020).

2.5. Heterotrophic respiration incubations

For the incubation experiment, soil samples were thawed and air-dried. 5 g from each soil sample were weighed in triplicate into 60 mL Qorpak vials, which were placed in 473 mL Mason jars along with a 20 mL glass vial containing a CO_2 trap (15 mL KOH, 0.18 M) made with CO_2 -free deionized water. CO_2 -free deionized water (5 mL) was added to the bottom of the jar to maintain a humid atmosphere. To account for the small amount of

CO_2 present in the jar, measurements from blank jars with no soil were used. Samples were hydrated to a moisture level equivalent to 50% of water-filled pore space with deionized water and incubated for 53 days at 20°C in the dark. On days 2, 7, 18, 33, and 53, the jars were opened, and the electrical conductivity of the KOH solutions was determined. After each measurement, the CO_2 traps were replaced with new KOH solutions in new vials, and fresh deionized water was added to the bottom of the jar. At each sampling event, the average ($n = 3$) electrical conductivity value of the KOH solution from the blank jars was subtracted from each jar's KOH electrical conductivity value. This corrected value was then converted into the volume of CO_2 released by the sample using a standard curve and further converted to mass $\text{CO}_2\text{-C}$ by applying the ideal gas law. The standard calibration curve was made by injecting known volumes of 99.99% CO_2 (Airgas, Inc, Elmira, NY) into septa-lidded Mason jars containing empty Qorpak vials, CO_2 traps, and 5 mL CO_2 -free water on the bottom. The electrical conductivity of the KOH solution was measured 24 hours after injection. Cumulative respiration was reported per unit soil (termed mineralization; mg $\text{CO}_2\text{-C/g}$ soil) and per unit SOC (termed mineralizability; mg $\text{CO}_2\text{-C/g}$ SOC). Microbial metabolic quotient (ng $\text{CO}_2\text{-C}/\mu\text{g}$ microbial biomass C-h) of each soil was calculated by dividing cumulative CO_2 after seven days of incubation by the microbial biomass C (Anderson and Domsch, 1993).

2.6. Statistical methods

All statistical analyses were done in R (Version 4.04). Linear regression models were constructed using the *lm* function with normalized moisture as the explanatory variable and the following response variables: %C, %N, $\delta^{13}\text{C}$, $\delta^{15}\text{N}$, and C:N in soil and soil fractions, the relative mass of soil fractions, microbial biomass C, dissolved organic C, Al and Fe concentrations in different extractions, and above- and belowground biomass. The effects of normalized moisture value and soil fraction on some response variables were analyzed using ANOVA, followed by Tukey's HSD post hoc test to determine significant differences between treatments. Pearson's correlation matrix was plotted using the *corrplot* package. Partial least squares (PLS) regression models were constructed using the *mdatools* package to identify the variables that best explain SOC content, mineralization, and mineralizability. PLS regression models reduce dimensionality and create components that maximize the covariance between predictor and response variables. As such, PLS models are advantageous in datasets that contain a similar number of predictor variables and observations and/or when predictors are highly correlated. Selectivity Ratio and Variable Importance in Projection tests were used to inform variable selection (See [Supplementary Material](#) for details on the variables selected for each model). The best model was selected according to the best goodness of fit, which was evaluated based on the highest cross-validated R^2 (R_{cv}^2), and lowest root mean of square error (RMSE).

3. RESULTS

3.1. Soil organic matter fractions

SOC and total nitrogen (TN) content increased with increasing normalized moisture value ($R^2 = 0.228$, $P = 0.019$, and $R^2 = 0.249$, $P = 0.014$, respectively) (Fig. 1). The relative amounts of oPOM and MAOM (g fraction/100 g soil) increased with increasing normalized moisture value ($R^2 = 0.178$, $P = 0.033$, and $R^2 = 0.442$, $P < 0.001$, respectively), but fPOM relative amount did not ($P = 0.9$) (Fig. 1). However, the proportion of total C in each fraction (mg/g SOC) did not differ across normalized moisture values (Fig. S3).

C:N ratios decreased in the order of roots > shoots > fPOM > oPOM > MAOM \approx bulk soil but were not significantly different across normalized moisture values (Fig. S4 and Table S2), apart from the C:N ratio of MAOM, which significantly decreased with increasing soil moisture level ($R^2 = 0.267$, $P = 0.011$) (Fig. 2A). The $\delta^{13}\text{C}$ values (mean \pm sd) in the bulk soil ($-27.5 \pm 0.3\text{‰}$) and MAOM ($-27.4 \pm 0.3\text{‰}$) fractions were significantly higher than those of the fPOM ($-28.4 \pm 0.5\text{‰}$) and oPOM ($-28.8 \pm 0.4\text{‰}$) fractions and plant biomass ($P < 0.0001$), though the interaction of normalized moisture and fraction on $\delta^{13}\text{C}$ was not significant (Fig. S5, Table S2). Additionally, $\delta^{13}\text{C}$ values of fPOM, oPOM, MAOM fractions and bulk soils decreased with increasing normalized moisture

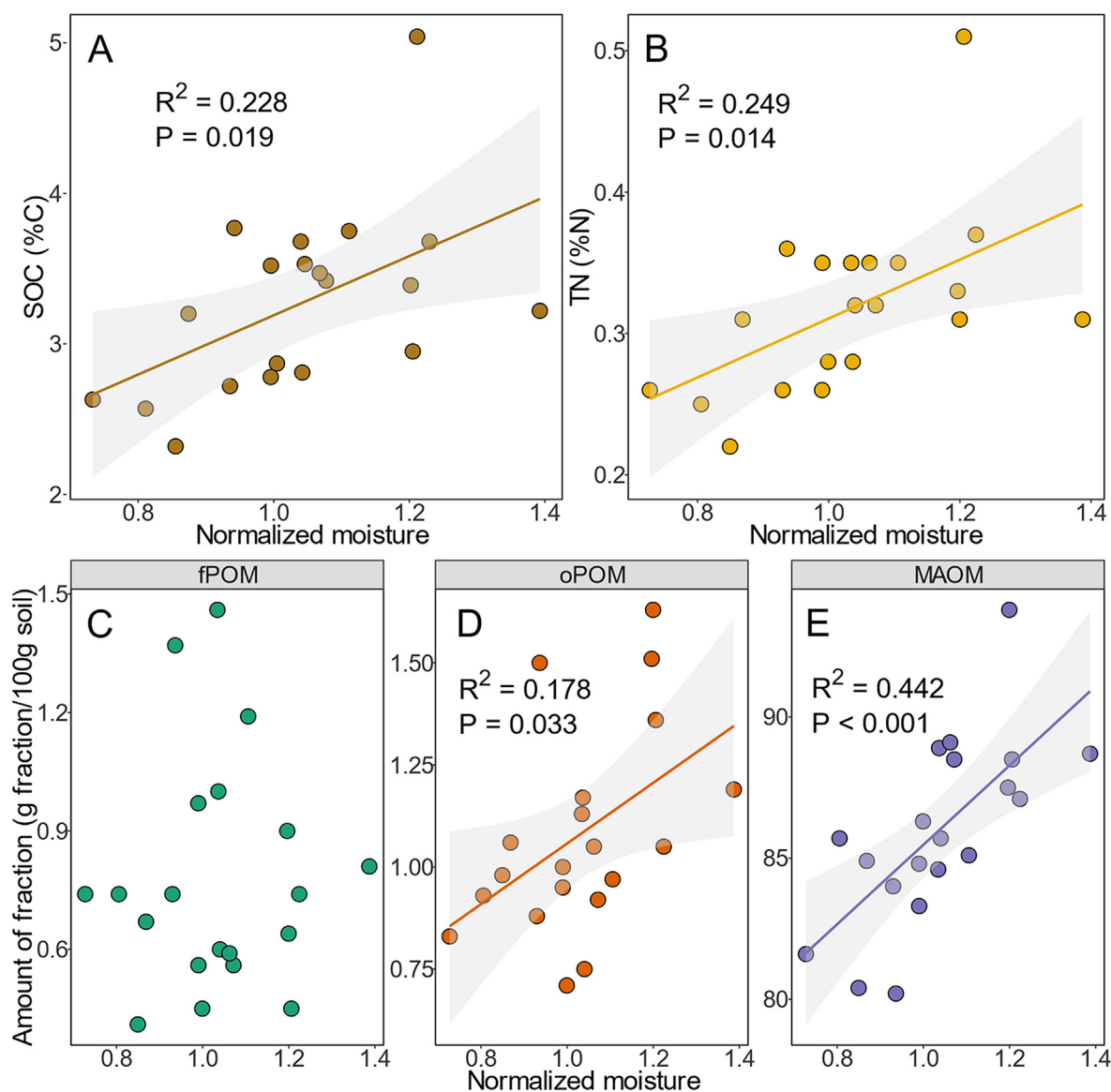


Fig. 1. Soil organic carbon (SOC) (A) and total nitrogen (TN) (B) contents, relative amount of free and occluded particulate organic matter fractions (fPOM and oPOM) (C, D), and mineral associated organic matter (MAOM) fraction (E), as a function of normalized soil moisture. Lines indicate significant linear regressions ($P < 0.05$).

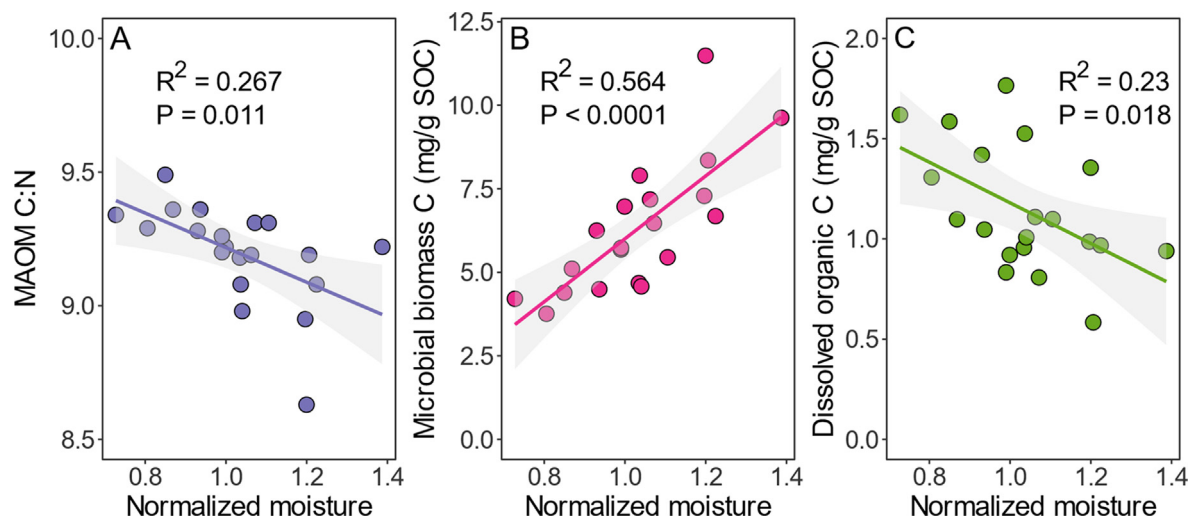


Fig. 2. C:N ratio of the mineral-associated organic matter (MAOM) (A), microbial biomass C (B), and dissolved organic C (C) (both normalized to SOC content) as a function of normalized soil moisture. Lines indicate significant linear regressions ($P < 0.05$).

values (Fig. S5). Normalized soil moisture or its interaction with soil fraction did not significantly affect $\delta^{15}\text{N}$ values (Fig. S6, Table S2).

3.2. Microbial biomass

Microbial biomass C increased with increasing normalized soil moisture, even when normalized to unit mass SOC ($R^2 = 0.564$, $P < 0.0001$), while dissolved organic C (DOC), as a proportion of SOC, decreased with increasing soil moisture ($R^2 = 0.230$, $P = 0.018$) (Fig. 2). Overall, DOC and microbial biomass C constituted up to 0.1% and 1% of the SOC, respectively.

3.3. Oxide extraction

The relative concentration of Al in each extract was similar across normalized soil moisture values (Fig. 3A). However, the relative concentration of Fe in organic-metal complexes (Fe_{PY}) decreased with increasing normalized soil moisture ($R^2 = 0.330$, $P = 0.005$) and the relative Fe concentration in crystalline phases (Fe_{DITH}) increased with increasing normalized soil moisture ($R^2 = 0.443$, $P = 0.001$) (Fig. 3B). We calculated the mass ratio of Al to Fe in each extract to further analyze these trends. In total, $\text{Al}_{\text{PY}}/\text{Fe}_{\text{PY}}$ and $\text{Al}_{\text{HH}}/\text{Fe}_{\text{HH}}$ increased with increasing normalized moisture ($R^2 = 0.287$, $P = 0.009$ for PY; $R^2 = 0.363$, $P = 0.003$ for HH), but $\text{Al}_{\text{DITH}}/\text{Fe}_{\text{DITH}}$ did not change (Fig. S8). In addition, the concentration of extracted OC increased as $\text{Al}_{\text{PY}}/\text{Fe}_{\text{PY}}$ and $\text{Al}_{\text{HH}}/\text{Fe}_{\text{HH}}$ increased, ($R^2 = 0.261$, $P = 0.013$ for PY; $R^2 = 0.182$, $P = 0.035$ for HH) (Fig. 3C), indicating that the increase in Al/Fe ratio in these extracts with increasing moisture (Fig. S8) was consistent with increasing OC. While the distribution of C across oxide pools varied with normalized moisture, the proportion of total oxide-associated C (which constituted on average 44% of the SOC) to SOC content

did not vary across normalized moisture values ($P = 0.79$, Fig. S9). Extractable Al was better correlated with OC_{PY} and OC_{HH} than Fe. Al_{PY} and Al_{HH} were significantly and positively correlated to OC in the respective extract ($R^2 = 0.513$; $P = 0.0002$, and $R^2 = 0.411$; $P = 0.0014$ respectively) (Fig. 3E) while Fe_{PY} and Fe_{HH} were not significantly correlated to extracted OC (Fig. 3D), consistent with the trends shown in Fig. S8 and Fig. 3C.

3.4. ATR-FTIR analysis

Bulk soil and MAOM spectra feature prominent bands assigned to Si–O stretching vibrations in quartz and clay minerals at 775, 795, and 1000 cm^{-1} , bands assigned to O–H and N–H stretching at around 3100–3500 cm^{-1} , and clay mineral structural hydroxyl groups at 3622 cm^{-1} (Fig. S10). fPOM and oPOM spectra featured O–H and N–H stretching around the broad band centered at 3350 cm^{-1} and bands assigned to asymmetric and symmetric stretching of aliphatic CH_2 at 2930 and 2855 cm^{-1} . Features originating from organic components (1250–1800 cm^{-1}) were less apparent in MAOM and bulk soil spectra (Fig. S10). To further investigate how differences in C:N ratios in the MAOM fractions were related to SOC composition, spectra of ashed MAOM samples were collected and subtracted from non-ashed MAOM spectra to reveal details of the organic constituents in the MAOM fraction. (Fig. 4). The spectra between 1250–1800 cm^{-1} consisted of bands tentatively assigned to stretching of C=O at 1645 cm^{-1} , COO^- and C=C at 1600 cm^{-1} , C=N, and bending N–H vibrations at 1545 cm^{-1} , and COO^- at 1420 cm^{-1} . We found higher absorbance in bands assigned to asymmetric and symmetric carboxylate COO^- stretch and amide/ketone C=O stretch (1420, 1600, and 1645 cm^{-1} , respectively), symmetric O–H stretching (3340 cm^{-1}), and asymmetric and symmetric CH_2 stretching

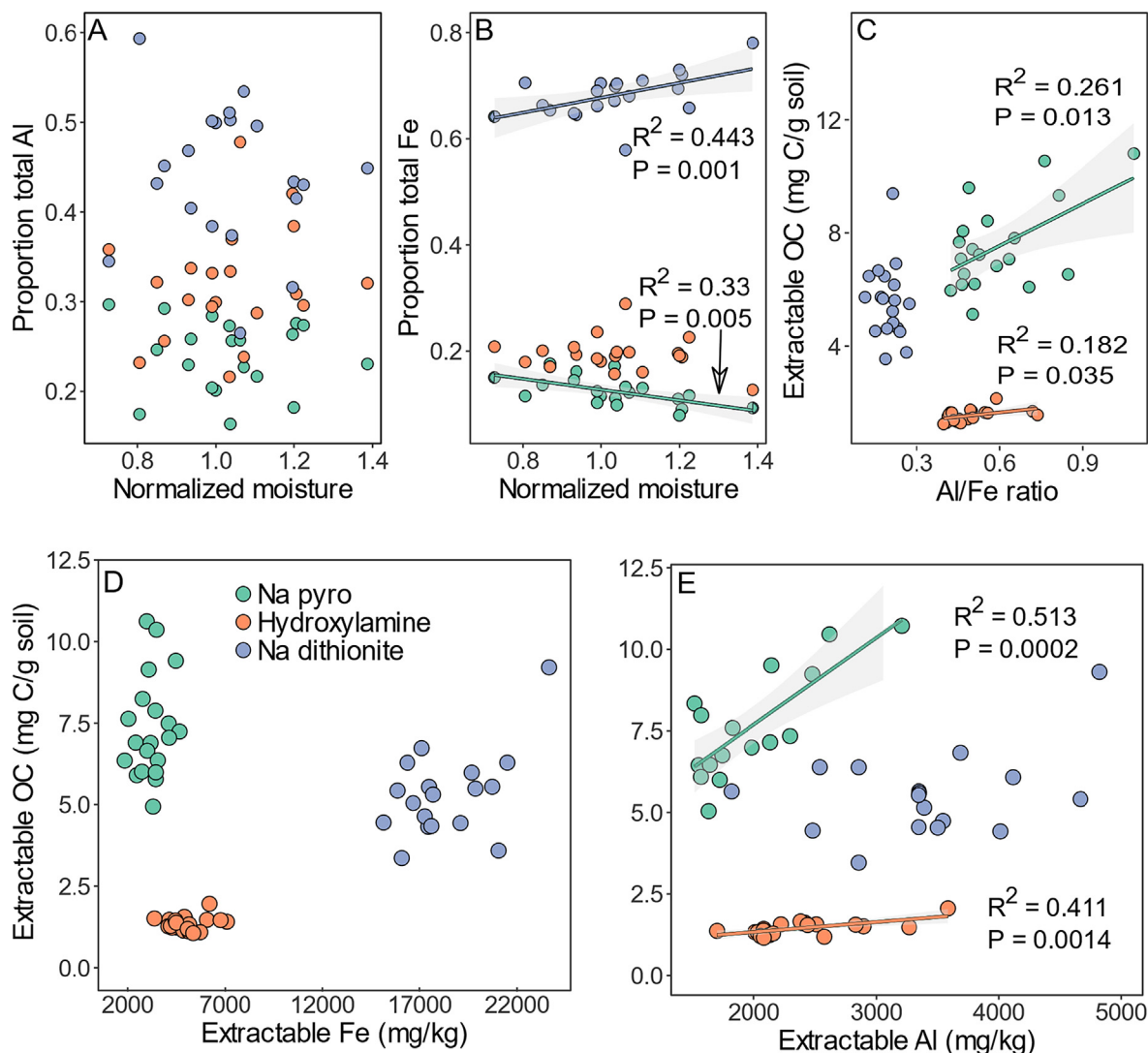


Fig. 3. Proportion of total extractable Al (A) and Fe (B), in sequential extractions of sodium pyrophosphate, hydroxylamine hydrochloride, and sodium dithionite, as a function of normalized soil moisture value. Extractable organic carbon (OC) as a function of Al/Fe ratio (C), extractable Fe (D), and Al (E) in the sequential extractions. Lines indicate significant linear regressions ($P < 0.05$).

(2930 and 2855 cm^{-1}) with increasing moisture level. Furthermore, there was a relative increase in the absorbance at 1545 cm^{-1} , assigned to stretching of aromatic C=N and bending of N-H.

3.5. ¹³C NMR analysis

In the MAOM fraction, the ratios of carboxyl-C/aromatic-C, carboxyl-C/O-alkyl-C, and O-alkyl-C/alkyl-C increased with increasing moisture level (Fig. 4C, Table S3). Comparing fractions, carboxyl-C and alkyl-C increased, and aromatic-C and O/N-alkyl-C decreased in the MAOM fraction compared to the fPOM and oPOM fractions (Fig. S11). According to the molecular mixing model, this shift echoes greater relative contents of carbohydrates and char in the fPOM and oPOM fractions compared to greater relative contents of proteinaceous and aliphatic compounds in MAOM and bulk soil (Fig. S12).

3.6. Carbon K – edge NEXAFS analysis

Confirming the ¹³C NMR results, we found that the ratio carboxyl C / (aromatic + substituted aromatic C) in the MAOM fractions, measured with C NEXAFS increased with increasing long term moisture level (Fig. 4D and Table S3). We did not evaluate changes in alkyl-C and O-alkyl-C forms since NEXAFS spectra did not have a strong and well-defined features corresponding to these bonding environments (Heckman et al., 2017). Overall, carboxyl-C forms relatively increased, while aromatic-C forms relatively decreased in the MAOM fraction relative to the fPOM and oPOM fractions (Fig. S13).

3.7. Soil heterotrophic respiration

Cumulative SOC mineralization after 53 days was positively correlated with normalized moisture values

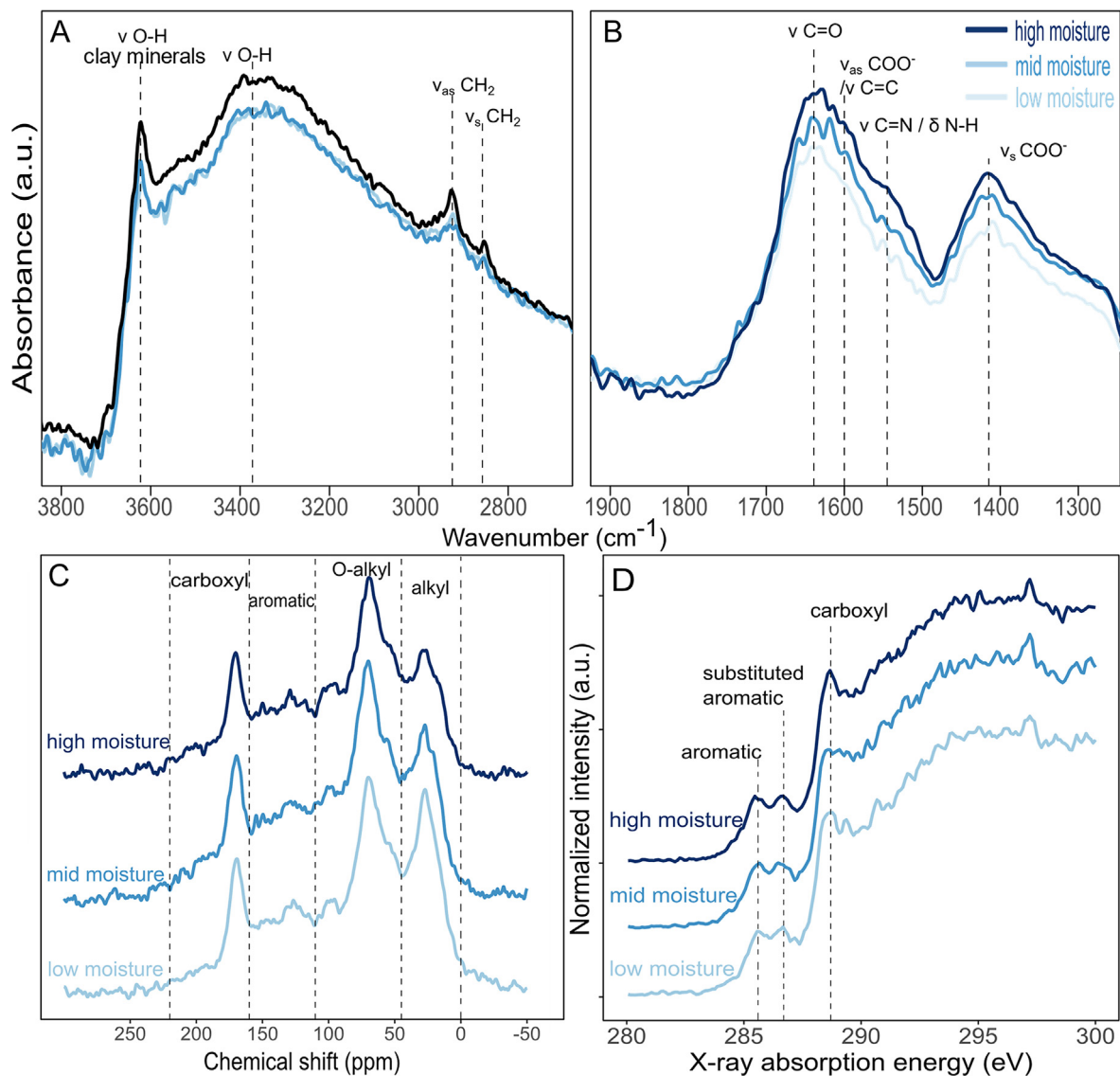


Fig. 4. Spectroscopic investigation of the chemical composition of mineral-associated organic matter (MAOM) fractions from low-, mid-, and high-moisture levels. ATR-FTIR spectra of ashed MAOM fractions ($n = 20$) subtracted from non-ashed MAOM samples ($n = 20$), highlighting the spectral features of SOC and differentiating them from mineral bands. Spectra were averaged across the moisture levels. The information-poor spectral region of $2000\text{--}2800\text{ cm}^{-1}$ is omitted (A and B). ^{13}C NMR spectra of MAOM fractions of composited samples from each moisture level (C). Carbon K-edge near-edge X-ray absorption fine structure (NEXAFS) spectra of MAOM fractions of composited samples from each moisture level (D).

($R^2 = 0.346$, $P = 0.0037$) (Fig. 5A), but no significant relationship was found between SOC mineralizability (mineralization per unit SOC) and moisture values ($P = 0.68$) (data not shown). The microbial metabolic quotient was negatively correlated with normalized moisture values ($P < 0.001$, $R^2 = 0.557$) (Fig. 5B).

Pearson's correlation coefficients and partial least squares (PLS) regression coefficients for SOC content, mineralization, and mineralizability are presented in Fig. 6 and Table 1, respectively. SOC contents were highly positively correlated with Ca_{EX} ($r = 0.67$), Al_{PY} ($r = 0.65$), $\text{Al}_{\text{PY}}/\text{Fe}_{\text{PY}}$ ($r = 0.62$), and normalized moisture ($r = 0.52$), and negatively correlated with microbial metabolic quotient ($r =$

-0.38). Similarly, the PLS regression model ($R_{\text{cv}}^2 = 0.449$; $\text{RMSE}_{\text{cv}} = 0.439$) identified Al_{PY} , $\text{Al}_{\text{PY}}/\text{Fe}_{\text{PY}}$, Ca_{EX} , and moisture as positively associated with SOC contents. SOC mineralization was correlated with SOC ($r = 0.81$) and Ca_{EX} ($r = 0.7$), and negatively correlated with DOC ($r = -0.41$). We did not refer to the correlation between mineralization and metabolic quotient ($r = -0.41$) since the former is used to calculate the latter. The PLS model identified only SOC as positively associated with SOC mineralization ($R_{\text{cv}}^2 = 0.710$; $\text{RMSE}_{\text{cv}} = 0.106$). SOC mineralizability was positively correlated with MAOM ($r = 0.42$) and microbial biomass C ($r = 0.39$), and negatively correlated with C:N ($r = -0.49$), Al_{PY} ($r = -0.43$), and Fe_{PY} ($r = -0.42$).

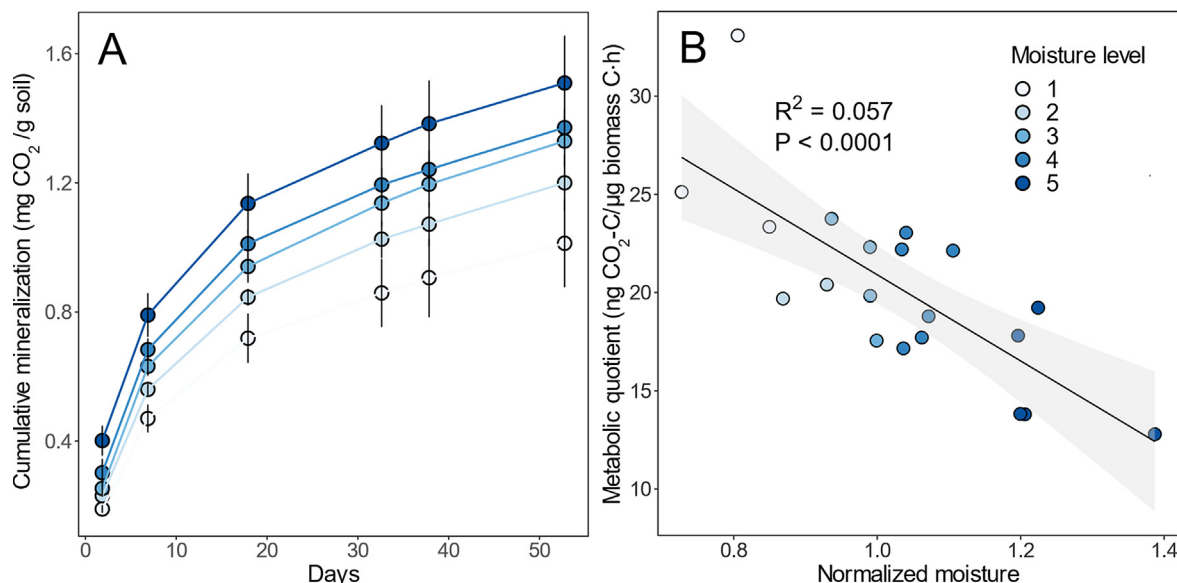


Fig. 5. Cumulative SOC mineralization during 53 days of incubation is plotted as means and standard errors for each moisture level (A) (See Table S1). Microbial metabolic quotient plotted as a function of normalized moisture value (B).

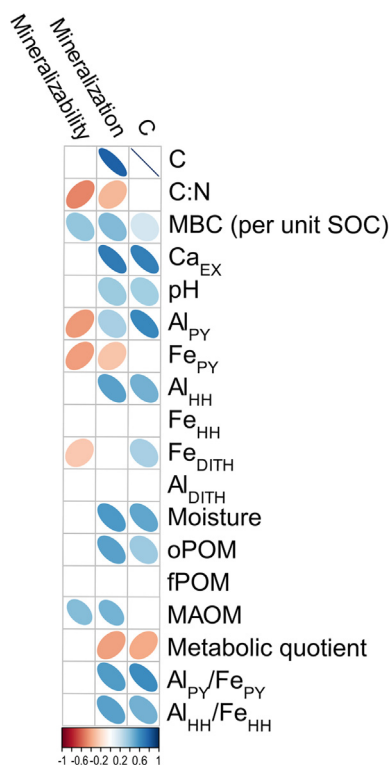


Fig. 6. Heatmap showing Pearson correlations (r) for selected variables with SOC content, mineralization, and mineralizability. Only significant ($P < 0.05$) correlations are plotted in the heatmap. The correlations between all variables are shown in Fig. S14.

Similarly, the PLS model identified Al_{py} and Fe_{py}, as negatively associated with SOC mineralizability, but overall model prediction was poor ($R^2_{cv} = 0.054$; $RMSE_{cv} = 1.852$).

4. DISCUSSION

4.1. Soil organic carbon accrual is unrelated to low microbial activity at high moisture

We found that SOC and TN increased with increasing long-term soil moisture in the fallow plots investigated in this study (Fig. 1A and 1B). This is consistent with previous work on this experimental site, which reported a similar trend, averaged over several cropping systems (Das et al., 2018). Here, we focused on the fallow plots to eliminate potential effects of the cropping system and to allow a direct investigation of the effects of long-term soil moisture on SOC dynamics. Enhanced SOC accumulation can result from greater inputs, smaller outputs, or both. Since above-ground and below-ground biomass were similar across the moisture gradient (Fig. S7), we argue that SOC accumulation resulted from reduced SOC output per unit C input.

While accumulation of SOC on seasonally saturated soils has been explained in terms of limited mineralization (O'Brien et al., 2010), our evidence suggests that this was not the case here. Measurements indicate that moisture in the wettest sites was lower than 80% water-filled pore space, i.e., less than saturated, in 82% of the growing season measurements taken over four years, from 2011 to 2014 (Das et al., 2019). A moisture level corresponding to 80% water-filled pore space can decrease heterotrophic respiration by approximately 10% from the maximum level (Moyano et al., 2012). Although we do not have detailed water content data for November through March, the existing data (and field observations) indicate that soil moisture is the greatest in these winter months. This is consistent with recent hydrological studies of the site (Brindt et al., 2022). Since SOC mineralization is expected to be the lowest during the winter regardless of water content,

Table 1

Results of partial least squares regression models. Coefficients are listed if they are statistically significant at $P < 0.05$ and bolded at $P < 0.001$. The coefficient of determination of the calibration (R_{cal}^2) and cross-validation sets (R_{cv}^2) and the root mean of square error (RMSE_{CV}) are provided.

	Moisture	SOC	Ca _{EX}	Al _{PY}	Fe _{PY}	Al _{PY} /Fe _{PY}	R_{cal}^2	R_{cv}^2	RMSE_{CV}
SOC	0.204	–	0.265	0.255	–	0.244	0.601	0.449	0.439
Mineralization	–	0.381	–	–	–	–	0.939	0.710	0.106
Mineralizability	–	–	–	–0.184	–0.148	–	0.387	0.054	1.852

saturation-driven limitation on mineralization was likely not important.

Furthermore, if mineralization of organic inputs was limited by high moisture, one might expect an impact on the decomposition trajectory of plant biomass to POM and MAOM fractions, resulting in a greater proportion of SOC remaining in the less processed POM fractions. However, our data show that the distribution of C (per unit SOC) among these fractions is similar across the moisture gradient (Fig. S3), indicating that organic matter mineralization followed a similar (and expected) decomposition trajectory in all the soils studied. We therefore suggest that the principal drivers of SOC accumulation were differences in SOC transformation and stabilization, mediated by microbial utilization of organic inputs and organo-mineral interactions with non-crystalline Al phases and Ca_{EX}-bearing minerals, and not due to transient oxygen limitation in saturated conditions that coincide with low mineralization during the winter months.

4.2. High long-term moisture increased microbial conversion of organic inputs into MAOM

Our results show a strong microbial biomass and DOC response to differences in long-term soil moisture (Fig. 2). Decreasing DOC (per unit SOC) and increasing microbial biomass C (per unit SOC) with increasing long-term moisture may have resulted from greater microbial oxidation of DOC, leading to enhanced interactions with minerals surfaces (Lehmann and Kleber, 2015), and ultimately to a decrease in DOC concentration. This hypothesis is supported by decreasing MAOM C:N values with increasing moisture, indicating more processed and oxidized microbial products. Furthermore, decreasing microbial metabolic quotient with increasing long-term moisture (Fig. 5B) indicates more efficient microbial use of C and less CO₂ emitted per unit biomass C.

MAOM fractions enriched in proteinaceous compounds, oxidized carboxylic-C, and O-alkyl-C functional groups, and depleted in alkyl-C and aromatic-C functional groups (Fig. 4, Table S3, Fig. S10, Fig. S11) indicated that high-moisture soils contained more products of microbial decomposition of aromatic and aliphatic plant residues, with concomitant enrichment in microbial proteinaceous components (Fig. S12). Taken together, our results clearly show that high long-term moisture led to greater oxidation and conversion of plant biomass into microbial biomass, which explains SOC accumulation.

4.3. Long-term moisture shaped mineral composition and C interactions with minerals

Our results reveal substantial differences in Fe phases across a narrow range of moisture conditions in which reducing conditions are a transient occurrence and unsaturated conditions predominate. Greater long-term moisture was associated with a 7% relative decrease in Fe_{PY}, which according to Mössbauer spectroscopy can comprise organic-Fe complexes and nanocrystalline Fe components (Thompson et al., 2011), and a 10% relative increase in crystalline Fe_{DITH} (Fig. 3B), resulting in increasing relative crystallinity of Fe phases. Crystalline Fe can be reduced in transient high moisture events through dissimilatory reduction (Pan et al., 2016) and subsequently be oxidized, forming non-crystalline precipitates which can contain large amounts of SOC (Chen et al., 2014b; Possinger et al., 2021). Fe reduction can occur in anaerobic microsites even as the bulk soil is under oxic conditions (Keiluweit et al., 2016). However, in the absence of subsequent protection through occlusion or surface coating, these Fe-C associations are vulnerable to dissolution when high moisture events reoccur (Chen et al., 2020a). Dissolution of the Fe-C association can lead to microbial decomposition of liberated C and loss of Fe from non-crystalline phases, resulting in increased Fe crystallinity (Thompson et al., 2006; Hodges et al., 2019; Possinger et al., 2020), which is consistent with our results (Fig. 3).

Al phases were not affected by moisture (Fig. 3A), likely because Al speciation is more pH-dependent than redox-dependent (Bertsch and Bloom, 2018). The loss of non-crystalline Fe, and likely the associated C, concomitantly with no changes in Al phases, resulted in increasing relative importance of Al_{PY} and Al_{HH} phases for C retention by soil oxides with increasing long-term moisture (Fig. 3C, 3E, and Fig. S8).

Several recent studies have similarly observed greater contribution of non-crystalline Al than Fe pools for SOC retention, albeit with greater saturation extent and frequency (Possinger et al., 2020) or annual higher precipitation (Inagaki et al., 2020). Indeed, a recent analysis of data from 2574 mineral horizons from National Ecological Observatory Network sites across North America showed that oxalate extractable non-crystalline Al was a better predictor of SOC storage than oxalate extractable Fe (Yu et al., 2021), suggesting that this effect was more common than previously thought. The interactions of C with different Al phases have received less attention than Fe-C

interactions. However, soil Al_{PY} phases and synthetic non-crystalline Al hydroxides preferentially interact with carboxylate groups (Parfitt et al., 1999; Guan et al., 2007). This is consistent with our spectroscopy analyses which show a greater proportion of carboxylic C, and other functional groups indicative of microbially processed compounds, in high-moisture MAOM fractions (Fig. 2 and Fig. 4). Because microbial products were more abundant at high moisture, the probability of organo-mineral interactions with these compounds increases. However, we cannot definitively determine the relative contribution of microbial products vs. root exudates, which also contain small, oxidized compounds. Considering the mounting evidence for the critical role of Al in SOC storage at a wide range of moisture conditions, we suggest that future research investigate the composition of SOC associated with Al, and the processes that influence the persistence of this important SOC pool.

Greater long-term moisture was also positively correlated with Ca_{EX} and pH (Fig. S15). Ca, in turn, was highly correlated with SOC ($r = 0.67$) (Fig. S14), indicating that increased Ca_{EX} in high-moisture soils contributed to SOC accrual, likely through cation-bridging of carboxylate functional groups (Fig. 4) (Rowley et al., 2018). While Ca and non-crystalline Fe can form ternary structures with carboxylate groups (Sowers et al., 2018), our soils showed a negative correlation between Fe_{PY} and Ca_{EX} (Fig. S14), implying that ternary Ca-Fe-C structures were less important for SOC accrual in our study. The positive correlations between moisture, Ca_{EX}, and pH can be explained by: (1) dissolution of subsoil carbonates and upward migration of Ca²⁺ ions facilitated by capillary rise in the high moisture soils (Ap horizon soils in this study did not have measurable calcium carbonate contents) (Das et al., 2019), and/or (2) greater contents of clay minerals containing Ca_{EX} due to lateral flow and deposition of fine-grained particles in shallower and wetter locations in the field (Das et al., 2018). Taken together, greater long-term moisture drove SOC accrual through an increase in Ca-bearing fine particles.

4.4. Long-term moisture regulates SOC accrual through microbial activity and mineral composition

SOC accrual in high moisture soils resulted from an interplay between soil moisture and biotic and abiotic processes. High long-term soil moisture enhanced microbial oxidation of organic inputs and concomitantly increased the relative content of non-crystalline Al phases and Ca_{EX}-bearing minerals, which in turn interact with the oxidized organic compounds (Fig. 4, Fig. 6, and Table 1). These conclusions are consistent with and extend the MEMS framework (Cotrufo et al., 2013), which explains SOC dynamics as a complex interaction between microbial efficiency for processing organic inputs and the capacity of soil minerals to stabilize these processed inputs.

Decreasing maintenance respiration (metabolic quotient) with increasing long-term moisture (Fig. 5B) indicates

lower CO₂ losses per unit C mineralized in high moisture soils, which is consistent with SOC accrual (Fig. 1 and Fig. 6). A lower metabolic quotient is often discussed in terms of reduced stress (Anderson and Domsch, 1993), and in the context of soil, moisture effects can be explained by reduced diffusional constraints, which improve the mobility of substrates and enzymes, leading to more efficient metabolism (Moyano et al., 2012; Roller and Schmidt, 2015). Similar conclusions were recently reported by Butcher et al. (2020), who found in laboratory experiments that decreased carbon use efficiency at low soil water contents was due to limited substrate diffusion. The volumetric water content of the low-moisture soils was on average 10% lower than that of the high-moisture soils (Fig. S2), which likely decreased substrate diffusion. Interestingly, our results were obtained from incubation experiments in which all soils were first air-dried and then hydrated to the same water-filled pore space, suggesting that long-term moisture exerted a sustained effect on microbial metabolic quotient, possibly through community composition structuring under various moisture regimes (Evans and Wallenstein, 2012; Banerjee et al., 2016). However, detailed examination of the microbial community composition was beyond the scope of this study. Our observations suggest that soil moisture can shape SOC accrual by its effects on microbial metabolic quotient. More work is needed to understand if we can manage soil moisture for optimized microbial efficiency and increased SOC stocks.

The superposition of microbial activity and an abundance of non-crystalline Al phases and Ca_{EX} acted to enrich high moisture MAOM fractions in carboxylate-rich compounds, consistent with other studies on Al-C and Ca-C interactions (Parfitt et al., 1999; Mouvenchery et al., 2012; Chen et al., 2014a; Rowley et al., 2018; Possinger et al., 2020; Wan et al., 2021). Interactions between carboxylates and cations are expected to prevail in the high moisture soils since the high pH found in them promotes electrostatic interactions between oppositely charged moieties. The contribution of Al_{PY} and Ca_{EX} to SOC content and the prevalence of carboxylic C in MAOM fractions (Fig. 4, Table S3, Fig. S12) suggest that organo-mineral interactions with microbially processed compounds were important for SOC accrual in the high moisture soils. MAOM and SOC contents were weakly correlated ($r = 0.19$; $P = 0.051$), indicating that specific effects of Ca_{EX}, rather than greater contents of silt- and clay-sized particles, played a role (Table 1, Fig. 6, and Fig. S14), likely due to the similar silt and clay contents in the studied soils.

Interestingly, the measured soil variables enabled poor prediction of mineralizability (mineralization per unit C) ($R^2_{CV} = 0.054$), indicating that the observed variation in soil chemical and mineral composition did not significantly influence the persistence of C in any given soil. The contribution of organo-mineral interactions to SOC accrual was therefore not due to a greater strength of interaction, decreased mineralizability, or longer turnover times of organic compounds interacting with a given mineral phase, as suggested by previous studies on pure minerals

(Sanderman et al., 2014; Newcomb et al., 2017), or soils of varying mineral composition (Mikutta et al., 2006; Khomo et al., 2017). The soil mineral composition in the current study was likely not dramatically different to the extent that organo-mineral interactions across the moisture gradient exerted observably different SOC stabilization. SOC accrual under high long-term moisture resulted from the more efficient conversion of plant input into microbial biomass through reduced C losses as CO₂, and a greater abundance of non-crystalline oxide phases and Ca-bearing minerals that protected the microbial products.

5. CONCLUSIONS

In the trade-off between mineralization and accrual, high long-term moisture increased SOC accrual, even at a soil moisture range not expected to constrain decomposition or alter soil oxide composition, indicating that such changes are likely to occur even along moderate soil moisture gradients. While the mechanism presented here may commonly occur in soils, the direction and magnitude of changes to SOC stocks under changing long-term soil moisture are likely to depend on additional soil properties that affect the microbial conversion of organic inputs and mineral interactions with these products. Additional studies on long-term soil moisture differences at numerous sites are necessary to elucidate these factors. For example, soils that do not have the mineral capacity to interact with oxidized organic compounds may not benefit from greater long-term moisture. Climate change is changing soil moisture and critically altering the magnitude and temporal patterns of moisture variability through extreme floods and droughts. The relative roles of mean long-term moisture vs. temporal variability of moisture on stabilization mechanisms are still not clear. Currently, conventional C models consider soil moisture as a physical variable only, and models that account for microbial traits do not include the potential effect of moisture on carbon use efficiency. These processes will have to be clarified to maintain SOC stocks by stabilizing organic inputs.

Declaration of Competing Interest

The authors declare that they have no known competing financial interests or personal relationships that could have appeared to influence the work reported in this paper.

ACKNOWLEDGEMENTS

This research was supported by BARD, the United States – Israel Binational Agricultural Research and Development Fund, Vaadia-BARD Postdoctoral Fellowship Award No. FI-573-2018, and the U.S. Department of Energy, Office of Biological & Environmental Research Genomic Science Program Award No. DE-SC0016364. Field research and moisture measurements have been supported by the US Department of Agriculture/National Institute for Food and Agriculture Grant No. 2011-67009-20083 and from Federal Capacity (Hatch) Project No. NYC-123486. Above ground biomass data were provided by the Department of Plant Breeding and Genetics, Cornell University.

APPENDIX A. SUPPLEMENTARY MATERIAL

Supplementary data to this article can be found online at <https://doi.org/10.1016/j.gca.2022.04.028>.

REFERENCES

- Anderson T. H. and Domsch K. H. (1993) The metabolic quotient for CO₂ (qCO₂) as a specific activity parameter to assess the effects of environmental conditions, such as pH, on the microbial biomass of forest soils. *Soil Biol. Biochem.* **25**, 393–395.
- Banerjee S., Helgason B., Wang L., Winsley T., Ferrari B. C. and Siciliano S. D. (2016) Legacy effects of soil moisture on microbial community structure and N₂O emissions. *Soil Biol. Biochem.* **95**, 40–50.
- Berg A. and Sheffield J. (2018) Climate change and drought: the soil moisture perspective. *Curr. Clim. Chang. Reports* **4**, 180–191.
- Bertsch P. M. and Bloom P. R. (2018) Aluminum. *Methods Soil Anal. Part 3 Chem. Methods*, pp. 517–550.
- Brindt N., Pacenka S., Richards B. K., Das S., Schatz A. L., Stoof C. R., Worqlul A. W., Zimale A. F., Azzaino Z., Parlange Jean-Yve and Steenhuis T. S. (2022) Self-Organizing Hydrological Processes in Runoff Source Areas. *Catena* **211**, 1–12.
- Butcher K. R., Nasto M. K., Norton J. M. and Stark J. M. (2020) Physical mechanisms for soil moisture effects on microbial carbon-use efficiency in a sandy loam soil in the western United States. *Soil Biol. Biochem.* **150**, 107969.
- Chen C., Dynes J. J., Wang J., Karunakaran C. and Sparks D. L. (2014a) Soft X-ray spectromicroscopy study of mineral-organic matter associations in pasture soil clay fractions. *Environ. Sci. Technol.* **48**, 6678–6686.
- Chen C., Dynes J. J., Wang J. and Sparks D. L. (2014b) Properties of Fe-organic matter associations via coprecipitation versus adsorption. *Environ. Sci. Technol.* **48**, 13751–13759.
- Chen C., Hall S. J., Coward E. and Thompson A. (2020a) Iron-mediated organic matter decomposition in humid soils can counteract protection. *Nat. Commun.* **11**, 1–13.
- Chen Q., Niu B., Hu Y., Luo T. and Zhang G. (2020b) Warming and increased precipitation indirectly affect the composition and turnover of labile-fraction soil organic matter by directly affecting vegetation and microorganisms. *Sci. Total Environ.* **714**, 136787.
- Cotrufo M. F., Wallenstein M. D., Boot C. M., Deneff K. and Paul E. (2013) The Microbial Efficiency-Matrix Stabilization (MEMS) framework integrates plant litter decomposition with soil organic matter stabilization: Do labile plant inputs form stable soil organic matter?. *Glob. Chang. Biol.* **19**, 988–995.
- Courchesne F. and Turmel M. C. (2007) Extractable Al, Fe, Mn, and Si. In *Soil Sampling and Methods of Analysis* (eds. M. R. Carter and E. G. Gregorich). CRC Press, pp. 335–344.
- Das S., Richards B. K., Hanley K. L., Krounbi L., Walter M. F., Walter M. T., Steenhuis T. S. and Lehmann J. (2019) Lower mineralizability of soil carbon with higher legacy soil moisture. *Soil Biol. Biochem.* **130**, 94–104.
- Das S., Teuffer K., Stoof C. R., Walter M. F., Walter M. T., Steenhuis T. S. and Richards B. K. (2018) Perennial grass bioenergy cropping on wet marginal land: Impacts on soil properties, soil organic carbon, and biomass during initial establishment. *Bioenergy Res.* **11**, 262–276.
- DeCiucies S., Whitman T., Woolf D., Enders A. and Lehmann J. (2018) Priming mechanisms with additions of pyrogenic organic matter to soil. *Geochim. Cosmochim. Acta* **238**, 329–342.

- Doetterl S., Stevens A., Six J., Merckx R., Van Oost K., Casanova P. M., Casanova-Katny A., Muñoz C., Boudin M., Zagal V. E. and Boeckx P. (2015) Soil carbon storage controlled by interactions between geochemistry and climate. *Nat. Geosci.* **8**, 780–783.
- Evans S. E. and Wallenstein M. D. (2012) Soil microbial community response to drying and rewetting stress: Does historical precipitation regime matter?. *Biogeochemistry* **109**, 101–116.
- Falloon P., Jones C. D., Ades M. and Paul K. (2011) Direct soil moisture controls of future global soil carbon changes: An important source of uncertainty. *Global Biogeochem. Cycles* **25**, 1–14.
- Fine A. K., Schmidt M. P. and Martínez C. E. (2018) Nitrogen-rich compounds constitute an increasing proportion of organic matter with depth in Oi-Oe-Oa-A horizons of temperate forests. *Geoderma* **323**, 1–12.
- Friedlingstein P., Jones M. W., O'Sullivan M., Andrew R. M., Hauck J., Peters G. P., Peters W., Pongratz J., Sitch S., Le Quéré C., Bakker D. C. E., Canadell J. G., Ciais P., Jackson R. B., Anthoni P., Barbero L., Bastos A., Bastrikov V., Becker M., Bopp L., Buitenhuis E., Chandra N., Chevallier F., Chini L. P., Currie K. I., Feely R. A., Gehlen M., Gilfillan D., Gkritzalis T., Goll D. S., Gruber N., Gutekunst S., Harris I., Haverd V., Houghton R. A., Hurtt G., Ilyina T., Jain A. K., Joetzjer E., Kaplan J. O., Kato E., Klein G. K., Korsbakken J. I., Landschützer P., Lauvset S. K., Lefèvre N., Lenton A., Lienert S., Lombardozi D., Marland G., McGuire P. C., Melton J. R., Metz N., Munro D. R., Nabel J. E. M. S., Nakaoka S.-I., Neill C., Omar A. M., Ono T., Peregona A., Pierrot D., Poulter B., Rehder G., Resplandy L., Robertson E., Rödenbeck C., Séférian R., Schwinger J., Smith N., Tans P. P., Tian H., Tilbrook B., Tubiello F. N., van der Werf G. R., Wiltshire A. J. and Zaehele S. (2019) Global Carbon Budget 2019. *Earth Syst. Sci. Data* **11**, 1783–1838.
- Ghezzehei T. A., Sulman B., Arnold C. L., Bogie N. A. and Asefaw B. A. (2019) On the role of soil water retention characteristic on aerobic microbial respiration. *Biogeosciences* **16**, 1187–1209.
- Grillakis M. G. (2019) Increase in severe and extreme soil moisture droughts for Europe under climate change. *Sci. Total Environ.* **660**, 1245–1255.
- Guan X., Hon, Chen G., Ha and Shang C. (2007) ATR-FTIR and XPS study on the structure of complexes formed upon the adsorption of simple organic acids on aluminum hydroxide. *J. Environ. Sci.* **19**, 438–443.
- Hall S. J., Berhe A. A. and Thompson A. (2018) Order from disorder: Do soil organic matter composition and turnover covary with iron phase crystallinity?. *Biogeochemistry* **140**, 93–110.
- Heckman K., Lawrence C. R. and Harden J. W. (2018) A sequential selective dissolution method to quantify storage and stability of organic carbon associated with Al and Fe hydroxide phases. *Geoderma* **312**, 24–35.
- Heckman K., Torres D., Swanston C. and Lehmann J. (2017) Carbon and nitrogen molecular composition of soil organic matter fractions resistant to oxidation. *Soil Res.* **55**, 809–818.
- Heymann K., Lehmann J., Solomon D., Schmidt M. W. I., Regier T., Lehmann J. J., Solomon D., Schmidt M. W. I. and Regier T. (2011) C 1s K-edge near edge X-ray absorption fine structure (NEXAFS) spectroscopy for characterizing functional group chemistry of black carbon. *Org. Geochem.* **42**, 1055–1064.
- Hodges C., Mallard J., Markewitz D., Barcellos D. and Thompson A. (2019) Seasonal and spatial variation in the potential for iron reduction in soils of the Southeastern Piedmont of the US. *Catena* **180**, 32–40.
- Huang W. and Hall S. J. (2017) Elevated moisture stimulates carbon loss from mineral soils by releasing protected organic matter. *Nat. Commun.* **8**, 1–10.
- Inagaki T. M., Possinger A. R., Grant K. E., Schweizer S. A., Mueller C. W., Derry L. A., Lehmann J. and Kögel-Knabner I. (2020) Subsoil organo-mineral associations under contrasting climate conditions. *Geochim. Cosmochim. Acta* **270**, 244–263.
- Kaiser K. and Zech W. (1996) Defects in estimation of aluminum in humus complexes of podzolic soils by pyrophosphate extraction. *Soil Sci.* **161**, 452–458.
- Keiluweit M., Nico P. S., Kleber M. and Fendorf S. (2016) Are oxygen limitations under recognized regulators of organic carbon turnover in upland soils?. *Biogeochemistry* **127**, 157–171.
- Khomo L., Trumbore S., Bern C. R. and Chadwick O. A. (2017) Timescales of carbon turnover in soils with mixed crystalline mineralogies. *Soil* **3**, 17–30.
- Kleber M., Bourg I. C., Coward E. K., Hansel C. M., Myneni S. C. B. and Nunan N. (2021) Dynamic interactions at the mineral-organic matter interface. *Nat. Rev. Earth Environ.* **0123456789**, 1–19.
- Knicker H. and Lüdemann H. D. (1995) N-15 and C-13 CPMAS and solution NMR studies of N-15 enriched plant material during 600 days of microbial degradation. *Org. Geochem.* **23**, 329–341.
- Kramer M. G. and Chadwick O. A. (2018) Climate-driven thresholds in reactive mineral retention of soil carbon at the global scale. *Nat. Clim. Chang.* **8**, 1104–1108.
- Kramer M. G., Sanderman J., Chadwick O. A., Chorover J. and Vitousek P. M. (2012) Long-term carbon storage through retention of dissolved aromatic acids by reactive particles in soil. *Glob. Chang. Biol.* **18**, 2594–2605.
- Lehmann J., Kinyangi J. and Solomon D. (2007) Organic matter stabilization in soil microaggregates: Implications from spatial heterogeneity of organic carbon contents and carbon forms. *Biogeochemistry* **85**, 45–57.
- Lehmann J. and Kleber M. (2015) The contentious nature of soil organic matter. *Nature* **528**, 60–68.
- Manzoni S., Taylor P., Richter A., Porporato A. and Ågren G. I. (2012) Environmental and stoichiometric controls on microbial carbon-use efficiency in soils. *New Phytol.* **196**, 79–91.
- Masiello C. A., Chadwick O. A., Southon J., Torn M. S. and Harden J. W. (2004) Weathering controls on mechanisms of carbon storage in grassland soils. *Global Biogeochem. Cycles* **18**, 1–9.
- Mikutta R., Kleber M., Torn M. S. and Jahn R. (2006) Stabilization of soil organic matter: Association with minerals or chemical recalcitrance?. *Biogeochemistry* **77**, 25–56.
- Mikutta R., Schaumann G. E., Gildemeister D., Bonneville S., Kramer M. G., Chorover J., Chadwick O. A. and Guggenberger G. (2009) Biogeochemistry of mineral-organic associations across a long-term mineralogical soil gradient (0.3–4100 kyr), Hawaiian Islands. *Geochim. Cosmochim. Acta* **73**, 2034–2060.
- Minasny B., Malone B. P., McBratney A. B., Angers D. A., Arrouays D., Chambers A., Chaplot V., Chen Z. S., Cheng K., Das B. S., Field D. J., Gimona A., Hedley C. B., Hong S. Y., Mandal B., Marchant B. P., Martin M., McConkey B. G., Mulder V. L., O'Rourke S., Richer-de-Forges A. C., Odeh I., Padarian J., Paustian K., Pan G., Poggio L., Savin I., Stolbovoy V., Stockmann U., Sulaeman Y., Tsui C. C., Vågen T. G., van Wesemael B. and Winowiecki L. (2017) Soil carbon 4 per mille. *Geoderma* **292**, 59–86.
- Mouvenchery Y. K., Diehl D. and Schaumann G. E. (2012) Cation-mediated cross-linking in natural organic matter: a review. *Rev. Environ. Sci. Biotechnol.* **11**, 41–54.

- Moyano F. E., Manzoni S. and Chenu C. (2013) Responses of soil heterotrophic respiration to moisture availability: An exploration of processes and models. *Soil Biol. Biochem.* **59**, 72–85.
- Moyano F. E., Vasilyeva N., Bouckaert L., Cook F., Craine J., Curiel Y. J., Don A., Epron D., Formanek P., Franzluebbers A., Ilstedt U., Kätker T., Orchard V., Reichstein M., Rey A., Ruamps L., Subke J. A., Thomsen I. K. and Chenu C. (2012) The moisture response of soil heterotrophic respiration: Interaction with soil properties. *Biogeosciences* **9**, 1173–1182.
- Nelson P. N. and Baldock J. A. (2005) Estimating the molecular composition of a diverse range of natural organic materials from solid-state ^{13}C NMR and elemental analyses. *Biogeochemistry* **72**, 1–34.
- Newcomb C. J., Qafoku N. P., Grate J. W., Bailey V. L. and De Yoreo J. J. (2017) Developing a molecular picture of soil organic matter-mineral interactions by quantifying organo-mineral binding. *Nat. Commun.* **8**, 1–8.
- O'Brien S. L., Jastrow J. D., Grimley D. A. and Gonzalez-Meler M. A. (2010) Moisture and vegetation controls on decadal-scale accrual of soil organic carbon and total nitrogen in restored grasslands. *Glob. Chang. Biol.* **16**, 2573–2588.
- Pan W., Kan J., Inamdar S., Chen C. and Sparks D. (2016) Dissimilatory microbial iron reduction release DOC (dissolved organic carbon) from carbon-ferrihydrite association. *Soil Biol. Biochem.* **103**, 232–240.
- Parfitt R. L. and Childs C. W. (1988) Estimation of forms of Fe and Al: A review, and analysis of contrasting soils by dissolution and moessbauer methods. *Aust. J. Soil Res.* **26**, 121–144.
- Parfitt R. L., Yuan G. and Theng B. K. G. G. (1999) A ^{13}C -NMR study of the interactions of soil organic matter with aluminium and allophane in podzols. *Eur. J. Soil Sci.* **50**, 695–700.
- Parikh S. J., Goyne K. W., Margenot A. J., Mukome F. N. D. D. and Calderón F. J. (2014) Soil chemical insights provided through vibrational spectroscopy. *Adv. Agron.* **126**, 1–148.
- Porras R. C., Hicks Pries C. E., McFarlane K. J., Hanson P. J. and Torn M. S. (2017) Association with pedogenic iron and aluminum: effects on soil organic carbon storage and stability in four temperate forest soils. *Biogeochemistry* **133**, 333–345.
- Possinger A. R., Bailey S. W., Inagaki T. M., Kögel-Knabner I., Dynes J. J., Arthur Z. A. and Lehmann J. (2020) Organo-mineral interactions and soil carbon mineralizability with variable saturation cycle frequency. *Geoderma* **375**, 1–14.
- Possinger A. R., Zachman M. J., Dynes J. J., Regier T. Z., Kourkoutis L. F. and Lehmann J. (2021) Co-precipitation induces changes to iron and carbon chemistry and spatial distribution at the nanometer scale. *Geochim. Cosmochim. Acta* **314**, 1–15.
- Rasmussen C., Heckman K., Wieder W. R., Keiluweit M., Lawrence C. R., Berhe A. A., Blankinship J. C., Crow S. E., Druhan J. L., Hicks Pries C. E., Marin-Spiotta E., Plante A. F., Schädel C., Schimel J. P., Sierra C. A., Thompson A. and Wagai R. (2018) Beyond clay: Towards an improved set of variables for predicting soil organic matter content. *Biogeochemistry* **137**, 297–306.
- Ravel B. and Newville M. (2005) ATHENA, ARTEMIS, HEPHAESTUS: Data analysis for X-ray absorption spectroscopy using IFEFFIT. *J. Synchrotron Radiat.* **12**, 537–541.
- Roller B. R. K. and Schmidt T. M. (2015) The physiology and ecological implications of efficient growth. *ISME J.* **9**, 1481–1487.
- Ross G. J., Wang C. and Schuppli P. A. (1985) Hydroxylamine and ammonium oxalate solutions as extractants for iron and aluminum from soils. *Soil Sci. Soc. Am. J.* **49**, 783–785.
- Rowley M. C., Grand S. and Verrecchia É. P. (2018) Calcium-mediated stabilisation of soil organic carbon. *Biogeochemistry* **137**, 27–49.
- Sanderman J., Maddern T. and Baldock J. (2014) Similar composition but differential stability of mineral retained organic matter across four classes of clay minerals. *Biogeochemistry* **121**, 409–424.
- Scharlemann J. P., Tanner E. V., Hiederer R. and Kapos V. (2014) Global soil carbon: Understanding and managing the largest terrestrial carbon pool. *Carbon Manag.* **5**, 81–91.
- Schjøning P., Thomsen I. K., Moldrup P. and Christensen B. T. (2003) Linking soil microbial activity to water- and air-phase contents and diffusivities. *Soil Sci. Soc. Am. J.* **67**, 156–165.
- Schuppli P. A., Ross G. J. and McKeague J. A. (1983) The effective removal of suspended materials from pyrophosphate extracts of soils from tropical and temperate regions. *Soil Sci. Soc. Am. J.* **47**, 1026–1032.
- Schurig C., Smittenberg R. H., Berger J., Kraft F., Woche S. K., Goebel M. O., Heipieper H. J., Miltner A. and Kaestner M. (2013) Microbial cell-envelope fragments and the formation of soil organic matter: A case study from a glacier forefield. *Biogeochemistry* **113**, 595–612.
- Seneviratne S. I., Corti T., Davin E. L., Hirschi M., Jaeger E. B., Lehner I., Orlowsky B. and Teuling A. J. (2010) Investigating soil moisture-climate interactions in a changing climate: A review. *Earth-Sci. Rev.* **99**, 125–161.
- Singh M., Sarkar B., Sarkar S., Churchman J., Bolan N., Mandal S., Menon M., Purakayastha T. J. and Beerling D. J. (2017) Stabilization of soil organic carbon as influenced by clay mineralogy. In *Advances in Agronomy*. Elsevier Inc., pp. 1–52.
- Solomon D., Lehmann J., Kinyangi J., Liang B., Heymann K., Dathe L., Hanley K., Wirick S. and Jacobsen C. (2009) Carbon (1s) NEXAFS spectroscopy of biogeochemically relevant reference organic compounds. *Soil Sci. Soc. Am. J.* **73**, 1817.
- Soong J. L., Castanha C., Hicks Pries C. E., Ofiti N., Porras R. C., Riley W. J., Schmidt M. W. I. and Torn M. S. (2021) Five years of whole-soil warming led to loss of subsoil carbon stocks and increased CO₂ efflux. *Sci. Adv.* **7**, 1–9.
- Sowers T. D., Adhikari D., Wang J., Yang Y. and Sparks D. L. (2018) Spatial associations and chemical composition of organic carbon sequestered in Fe, Ca, and organic carbon ternary systems. *Environ. Sci. Technol.* **52**, 6936–6944.
- Thompson A., Chadwick O. A., Rancourt D. G. and Chorover J. (2006) Iron-oxide crystallinity increases during soil redox oscillations. *Geochim. Cosmochim. Acta* **70**, 1710–1727.
- Thompson A., Rancourt D. G., Chadwick O. A. and Chorover J. (2011) Iron solid-phase differentiation along a redox gradient in basaltic soils. *Geochim. Cosmochim. Acta* **75**, 119–133.
- Todd-Brown K. E. O., Randerson J. T., Hopkins F., Arora V., Hajima T., Jones C., Shevliakova E., Tjiputra J., Volodin E., Wu T., Zhang Q. and Allison S. D. (2014) Changes in soil organic carbon storage predicted by Earth system models during the 21st century. *Biogeosciences* **11**, 2341–2356.
- Wagai R., Kajiura M. and Asano M. (2020) Iron and aluminum association with microbially processed organic matter via meso-density aggregate formation across soils: Organo-metallic glue hypothesis. *Soil* **6**, 597–627.
- Wagai R. and Mayer L. M. (2007) Sorptive stabilization of organic matter in soils by hydrous iron oxides. *Geochim. Cosmochim. Acta* **71**, 25–35.
- Wan D., Ma M., Peng N., Luo X., Chen W., Cai P., Wu L., Pan H., Chen J., Yu G. and Huang Q. (2021) Effects of long-term fertilization on calcium-associated soil organic carbon: Implications for C sequestration in agricultural soils. *Sci. Total Environ.* **772**, 145037.

- Wang S., Jia Y., Liu T., Wang Y., Liu Z. and Feng X. (2021) Delineating the role of calcium in the large-scale distribution of metal-bound organic carbon in soils. *Geophys. Res. Lett.* **48**, 1–11.
- Witt C., Gaunt J. L., Galicia C. C., Ottow J. C. G., Neue H. U. and Neue J. C. G. O. H. (2000) A rapid chloroform-fumigation extraction method for measuring soil microbial biomass carbon and nitrogen in flooded rice soils. *Biol. Fertil. Soils* **30**, 510–519.
- Wojdyr M. (2010) Fityk: a general-purpose peak fitting program. *J. Appl. Crystallogr.* **43**, 1126–1128.
- Yu W., Weintraub S. R. and Hall S. J. (2021) Climatic and geochemical controls on soil carbon at the continental scale: Interactions and thresholds. *Global Biogeochem. Cycles* **35**, 1–15.
- Zhao Q., Poulson S. R., Obrist D., Sumaila S., Dynes J. J., McBeth J. M. and Yang Y. (2016) Iron-bound organic carbon in forest soils: Quantification and characterization. *Biogeosciences* **13**, 4777–4788.
- Zhu X., Jackson R. D., DeLucia E. H., Tiedje J. M. and Liang C. (2020) The soil microbial carbon pump: From conceptual insights to empirical assessments. *Glob. Chang. Biol.* **26**, 6032–6039.

Associate editor: Elizabeth Herndon